Resolving the mass loss from red supergiants by high angular resolution

Keiichi Ohnaka

Instituto de Astronomía, Universidad Católica del Norte, Avenida Angamos 0610,
Antofagasta, Chile
e-mail: `k1.ohnaka@gmail.com`

Abstract. Despite its importance on late stages of the evolution of massive stars, the mass loss from red supergiants (RSGs) is a long-standing problem. To tackle this problem, it is essential to observe the wind acceleration region close to the star with high spatial resolution. While the mass loss from RSGs is often assumed to be spherically symmetric with a monotonically accelerating wind, there is mounting observational evidence that the reality is much more complex. I review the recent progress in high spatial resolution observations of RSGs, encompassing from the circumstellar envelope on rather large spatial scales (∼100 stellar radii) to milliarcsecond-resolution aperture-synthesis imaging of the surface and the atmosphere of RSGs with optical and infrared long-baseline interferometers.

Keywords. stars: mass loss, stars: imaging, stars: atmospheres, (stars:) supergiants, (stars:) circumstellar matter, infrared: stars, techniques: high angular resolution, techniques: interferometers, techniques: polarimetric

1. Introduction

The mass loss in the red supergiant (RSG) phase significantly affects the evolution of massive stars. For example, the RSG mass loss is considered to be a key to constraining the mass of the progenitors of supernovae (SNe) type IIP, which are the most common core-collapse SNe (e.g., Smartt 2015). Despite such importance, the mass loss from RSGs is one of the long-standing problems in stellar astrophysics. It is often argued that dust grains form in the atmosphere or in the circumstellar envelope of RSGs and the radiation pressure on the dust grains can drive the mass loss. However, it is not yet well understood where and how dust forms in RSGs, and it is possible that the mass loss is driven by some yet-to-be identified physical process. As Harper (2010) notes, there is no self-consistent theoretical model for the RSG mass loss at the moment.

High spatial resolution observations of RSGs provide us with valuable information to tackle the mass loss problem. However, even the closest RSG Betelgeuse has an angular diameter of only 42.5 mas (Ohnaka *et al.* 2011). This angular diameter is much smaller compared to the angular resolution of conventional ground-based imaging of ∼1″, which is limited by seeing. With adaptive optics, it is possible to achieve angular resolution corresponding to the diffraction limit of the telescope, which is 17 mas and 50 mas at 0.55 μm and 2 μm with an 8 m telescope, respectively. In the mid-infrared it is possible to achieve the diffraction limit (300 mas at 10 μm) without adaptive optics if the seeing is better than ∼0.6″ in the visible . This means that the structures of the circumstellar envelope of nearby RSGs on large spatial scales (∼100 stellar radii) can be resolved by diffraction-limited mid-infrared imaging. The diffraction-limited adaptive optics imaging in the visible and near-infrared can resolve the structures of the circumstellar environment close to the star, within several stellar radii. However, milliarcsecond angular resolution is required to spatially resolve the detailed structures of the wind acceleration region and
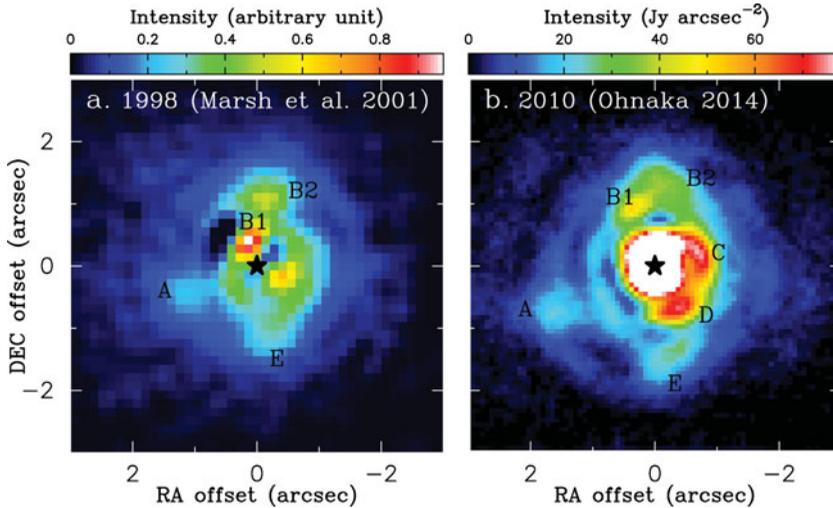
Figure 1. Clumpy dust clouds toward the RSG Antares detected in the mid-infrared. **a:** The 20.8 μm image obtained by Marsh *et al.* (2001). The central star is subtracted. **b:** The 17.7 μm image obtained by Ohnaka (2014) with the central star subtracted. The individual dust clouds are labeled. In both panels, the intensity is shown in the linear scale.

the stellar surface of RSGs, which is possible only by optical and infrared long-baseline interferometry.

2. Circumstellar envelope up to ∼100 stellar radii

It is often assumed that the stellar winds from RSGs are spherically symmetric and are monotonically accelerating until they reach terminal velocities of 20–40 km s^{-1}. The spatially resolved 4.6 μm CO emission of the prototypical RSG Betelgeuse shows an overall spherical envelope with mildly clumpy structures within 3″, which corresponds to 140 stellar radii (Smith *et al.* 2009). The mid-infrared imaging of Betelgeuse by Kervella *et al.* (2011) shows the clumpy structures more clearly. The images obtained from 7.76 to 19.5 μm show that the circumstellar envelope is approximately spherical within ∼1″ (∼47 stellar radii) but prominent clumpy structures. The images also show emission extending up to ∼2″ (∼94 stellar radii) in the south and northwest.

Ohnaka (2014) detected similar clumpy structures in the circumstellar envelope of another well-studied RSG, Antares, based on the diffraction-limited 17.7 μm image. As Fig. 1 (right) shows, the image reveals six clumpy dust clumps located at 0.8–1.8″ (43–96 stellar radii) and compact emission within 0.5″ (27 stellar radii) around the star. Moreover, comparison of this image taken in 2010 and the 20.8 μm image taken in 1998 by Marsh *et al.* (2001) (Fig. 1 left) shows the outward motions of the individual dust clouds. The observed proper motions of the dust clouds (with respect to the central star) of 0.2–0.6″ in 12 years translate into the velocities of 13–40 km s^{-1} projected onto the plane of the sky. The distances and velocities of the dust clouds may not be explained by a simple monotonically accelerating wind but suggest that the individual clouds may be ejected at different velocities from the beginning, although the projection effect does not allow us to draw a definitive conclusion.

While the mass loss from Betelgeuse and Antares is roughly spherically symmetric with small-scale clumpy structures superimposed, some RSGs show deviation from spherical
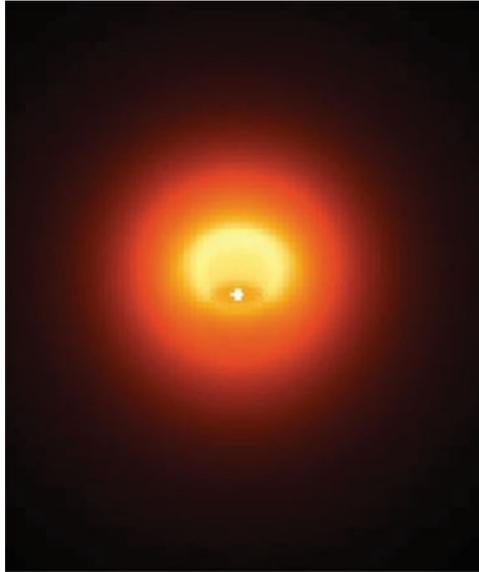
Figure 2. The 9 μm image predicted by the dust torus model of the RSG WOH G64 in the Large Magellanic Cloud (Ohnaka *et al.* 2008). The dust torus is seen nearly pole-on.

symmetry on large spatial scales. For example, the RSG μ Cep shows elongation on angular scales of 0.5 to 5″ (de Wit *et al.* 2008; Shenoy *et al.* 2016), while the extremely dusty RSG VY CMa shows a bipolar outflow with much more complex structures overlaid (Monnier *et al.* 1999; Smith *et al.* 2001).

High angular resolution observations also allow us to probe the morphology of the circumstellar envelope of RSGs beyond the Milky Way Galaxy. The mid-infrared (8–13 μm) interferometric observations of the RSG WOH G64 in the Large Magellanic Cloud using the MIDI instrument at the Very Large Telescope Interferometer (VLTI) were the first (and are still the only) study to spatially resolve an individual star in an extragalactic system (Ohnaka *et al.* 2008). The measured angular size (15–20 mas at 8 μm and ∼25 mas at 13 μm) does not show noticeable position angle dependence. The 2-D radiative transfer modeling of the interferometric data and the spectral energy distribution (SED) revealed the presence of a geometrically and optically thick dust torus seen nearly pole-on with an inner boundary radius of 15 ± 5 stellar radii (see Fig. 2). While the luminosity of WOH G64 previously estimated based on the spherical models suggested an initial mass of 40 $M_\odot$, the current evolutionary theory predicts that such a high mass star does not reach the RSG phase. However, the luminosity re-estimated with the presence of the dust torus taken into account is about a half of the previously estimated value. This newly estimated luminosity suggests an initial mass of 25 $M_\odot$, instead of 40 $M_\odot$, and brings the star's position on the H-R diagram in much better agreement with the evolution theory.

3. Circumstellar environment close to the star

To understand the origin of the clumpy structures seen in the circumstellar envelope, it is necessary to study the circumstellar environment close to the star, within several stellar radii. The advent of extreme adaptive optics combined with polarimetric imaging allows us to probe the circumstellar dust environment in great detail. With the unpolarized
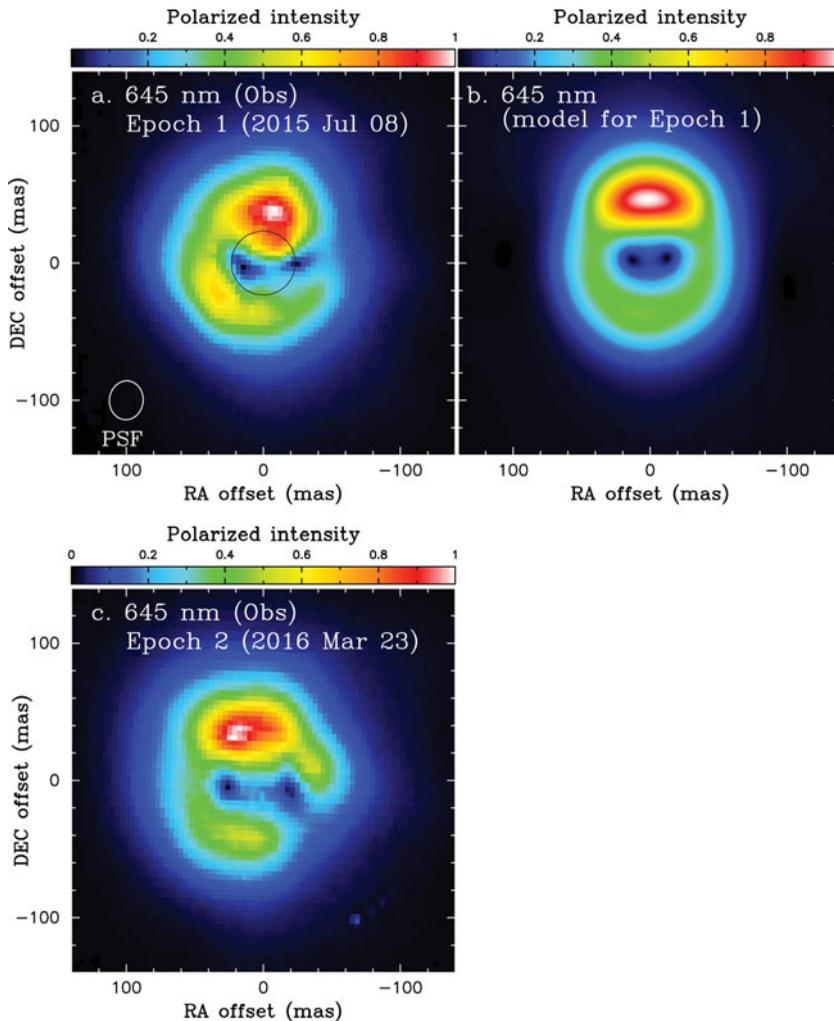
Figure 3. Clumpy dust clouds of the Mira star W Hya forming close to the photosphere detected with the VLT/SPHERE-ZIMPOL instrument (Ohnaka *et al.* 2016, 2017). **a:** Polarized intensity map obtained at 645 nm on 2015 July 8, when the star was at pre-maximum light. The black circle represents the size of the star measured with the VLTI/AMBER instrument. **b:** Model image at 645 nm for the 2015 data. **c:** Polarized intensity map obtained at 645 nm on 2016 March 23, when the star was at minimum light. In all panels, north is up, and east is to the left.

direct light from the bright central star is effectively suppressed, polarimetric imaging is very powerful for detecting faint scattered light from dust forming close to the star.

Ohnaka *et al.* (2016) observed the nearby, well-studied Mira star W Hya from 645 to 820 nm with the VLT/SPHERE-ZIMPOL instrument and detected clumpy dust clouds within ~50 mas (~2 stellar radii), revealing that dust formation takes place very close to the star (Fig. 3a). The clumpy dust formation may be induced by large convective cells as predicted by the 3-D simulations for AGB stars (Freytag & Höfner 2008). The Monte-Carlo radiative transfer modeling of the observed polarized intensity maps suggests the presence of an optically thin shell consisting of large (0.4–0.5 μm) grains of corundum (Al_2O_3), forsterite (Mg_2SiO_4), or enstatite ($MgSiO_3$), as shown in Fig. 3b. The inner

boundary radius of the shell is 1.9–2.0 stellar radii, where the dust temperature reaches 1500 K.

When these observations took place, the Mira star W Hya was at pre-maximum light, just before the brightest phase. The follow-up observations of W Hya reveal significant time variations in the morphology of the dust clouds. As shown in Fig. 3c, the polarized intensity map obtained 8.5 months later at minimum light shows the formation of a new dust cloud approximately in the west and the disappearance of the dust clouds in the southwest and southeast. The degree of linear polarization measured at minimum light, 13–18%, is noticeably higher than that observed at pre-maximum light. Interestingly, the Monte Carlo radiative transfer modeling shows that the minimum-light data can be explained by a shell of 0.1 μm grains of corundum, forsterite, or enstatite, in marked contrast to the large grain sizes of 0.4–0.5 μm found at pre-maximum light. Perhaps small grains might just have started to form at minimum light in the wake of a shock induced by the large-amplitude stellar pulsation, while the pre-maximum light phase might have corresponded to the phase of efficient grain growth.

Kervella *et al.* (2016) carried out visible polarimetric imaging observations of Betelgeuse with SPHERE-ZIMPOL and detected polarimetric signal resulting from dust scattering within three stellar radii. This suggests that dust forms close to the star in RSGs as well, which may play an important role in accelerating the stellar wind.

4. Imaging the surface and atmosphere of RSGs

Since Schwarzschild (1975) predicted that the convective cells on the surface of RSGs can be as large as the radius of the star, high spatial observations have been carried out to detect such large spots. Relatively recent observations include the aperture-synthesis image of Betelgeuse obtained at 1.6 μm by Haubois *et al.* (2009). They detected two spots, which have a size of 1/4–1/2 of the radius of the star with an intensity contrast of 5–10%. Monnier *et al.* (2014) present images of VY CMa reconstructed at 1.61, 1.67, and 1.73 μm from the data taken with the VLTI/PIONIER instrument. The images reveal an extended atmosphere elongated in the E-W direction and two bright spots with a size of the stellar radius on the stellar surface. Baron *et al.* (2014) present the 1.65 μm aperture-synthesis images of two RSGs, T Per and RS Per, in the Double Cluster obtained with the Center for High-Angular Resolution Astronomy (CHARA) array. While T Per shows a bright spot with a size comparable to the stellar radius, RS Per shows a large dark region near the limb. The contrast of the surface structures is approximately 15% in both cases. These spots are considered to represent large convective cells, which were predicted by Schwarzschild (1975) and modeled by 3-D convection simulations (e.g., Chiavassa *et al.* 2010). However, Montargès *et al.* (2016) show that the interferometric data of Betelgeuse obtained at 1.6 μm suggest surface structures more inhomogeneous and with a higher contrast than predicted by the 3-D convection simulations.

5. Velocity-resolved aperture-synthesis imaging of RSGs

If we combine milliarcsecond-resolution aperture-synthesis imaging with high spectral resolution, we can have a data cube over individual molecular or atomic lines. Then it is possible to extract the spatially resolved spectrum at each spatial position from the data cube. The spatially resolved spectra of individual lines allow us to measure the gas velocity at each position over the surface of stars as well as in the atmosphere, just as routinely done in solar observations.

Ohnaka *et al.* (2009) detected the signatures of inhomogeneous gas motions in the atmosphere of Betelgeuse based on the interferometric data obtained over the 2.3 μm CO lines with the VLTI/AMBER instrument with a spectral resolution of up to 12000. Ohnaka *et al.* (2011) present 1-D aperture-synthesis images of Betelgeuse in the individual CO lines with an angular resolution of 9.8 mas. The spectral resolution was high enough to have $\sim$10 wavelength points within each CO line profile. The 1-D images reconstructed in the blue wing and the line center of the CO line profiles show an atmosphere asymmetrically extending to $\sim$1.3 stellar radii. However, the 1-D images in the red wing do not show the extended component. The observed different appearance of the star across the CO line profiles can be explained by an inhomogeneous velocity field in the extended atmosphere. For example, we assume that a gas clump in front of the star is moving toward the observer (i.e., moving upward with respect to the star), while the gas outside the clump is moving away from the observer (i.e., moving downward). The gas clump in front of the star produces blueshifted absorption, while we expect redshifted absorption from the gas outside the clump. The modeling of Ohnaka *et al.* (2009, 2011) suggests vigorous upwelling and downdrafting motions of a gas clump as large as the radius of the star at velocities of 10–30 km s^{-1}. The spatially resolved spectra over the extended atmosphere extracted from the reconstructed data cube show prominent emission, while those inside the limb of the star show absorption, which is exactly what we expect from the Kirchhoff's law (Ohnaka 2013). Ohnaka *et al.* (2013) succeeded in spatially resolving a similar, inhomogeneous velocity field in Antares based on VLTI/AMBER data. These studies demonstrate that it is now feasible to map the 2-D velocity field from the wavelength shifts of the spatially resolved spectra in a straightforward manner.

One may attribute the vigorous, inhomogeneous motions observed in Betelgeuse and Antares to large convective cells. However, Ohnaka *et al.* (2013) demonstrate that the density of the extended atmosphere at 1.3 stellar radii estimated from the observed data is $\sim$10^{-14} g cm^{-3}, which is higher than that predicted by the current 3D convection simulations (Chiavassa *et al.* 2010) by 6 to 11 orders of magnitude. This means that the atmosphere of Betelgeuse and Antares extending to 1.3–1.5 stellar radii cannot be explained by convection alone. Arroyo-Torres *et al.* (2015) suggest that radiation pressure on molecular lines may drive the mass loss in RSGs, although it is still necessary to construct self-consistent models and compare to the observed data.

6. Prospects

A next step is to apply the velocity-resolved imaging to different atomic and molecular lines forming at different atmospheric heights. This enables us to obtain a 3-D view of the atmospheric dynamics. The "tomographic velocity-resolved aperture-synthesis imaging" is crucial for understanding how the energy and momentum needed to accelerate the stellar winds are transferred from the deep photosphere to the outer atmosphere.

The second generation VLTI instruments GRAVITY (Eisenhauer *et al.* 2008) and MATISSE (Lopez *et al.* 2014) will be important for further probing the wind acceleration of RSGs. The GRAVITY instrument, which operates between 2 and 2.4 μm and combines four telescopes, will allow us to carry out aperture-synthesis imaging much more efficiently, although its spectral resolution of 4000 is three times lower than that of AMBER. The MATISSE instrument, which will allow us to carry out aperture-synthesis imaging in the thermal infrared (3–13 μm) for the first time, is essential for directly probing the dust formation region. The combination of these high-angular resolution observations will provide us with a comprehensive picture of the complex atmosphere and

circumstellar envelope of RSGs and help us solve the long-standing problem of the mass loss.

References

Arroyo-Torres, B., Wittkowski, M., Chiavassa, A., *et al.* 2015, *A&A*, 575, A50

Baron, F., Monnier, J.D., Kiss, L.L., *et al.* 2014 *ApJ*, 785, 46

Chiavassa, A., Haubois, X., Young, J. S., *et al.* 2010, *A&A*, 515, A12

de Wit, W. J., Oudmaijer, R. D., Fujiyoshi, T., *et al.* 2008, *ApJ*, 685, L75

Eisenhauer, F., Perrin, G., Brandner, W., *et al.* 2008, *SPIE Proc.*, 7013, 70132A

Freytag, B. & Höfner, S. 2008, *A&A*, 483, 571

Harper, G. M. 2010, *ASP. Conf. Ser*, 425, 152

Haubois, X., Perrin, G., Lacour, S., *et al.* 2009, *A&A*, 508, 923

Kervella, P., Perrin, G., Chiavassa, A., *et al.* 2011, *A&A*, 531, A117

Kervella, P., Lagadec, E., Montargès, M., *et al.* 2016, *A&A*, 585, A28

Lopez, B., Lagarde, S., Jaffe, W., *et al.* 2014, *The Messenger*, 157, 5

Marsh, K. A., Bloemhof, E. E., Koerner, D. W., & Ressler, M. E. 2001, *ApJ* 548, 861

Monnier, J. D., Tuthill, P. G., Lopez, B., *et al.* 1999, *ApJ*, 512, 351

Monnier, J. D., Berger, J.-P., Le Bouquin, J.-B., *et al.* 2014, *SPIE Proc*, 9146, 91461Q

Montargès, M., Kervella, P., Perrin, G., *et al.* 2016, *A&A*, 588, A130

Ohnaka, K. 2013, *EAS Publications Series*, 60, 121

Ohnaka, K. 2014, *A&A*, 568, A17

Ohnaka, K., Driebe, T., Hofmann, K.-H., Weigelt, G., & Wittkowski, M. 2008, *A&A*, 484, 371

Ohnaka, K., Hofmann, K.-H., Benisty, M., *et al.* 2009, *A&A*, 503, 183

Ohnaka, K., Weigelt, G., Millour, F., Hofmann, K.-H., Driebe, T., Schertl, D., Chelli, A., Massi, F., Petrov, R., & Stee, Ph. 2011, *A&A*, 529, A163

Ohnaka, K., Hofmann, K.-H., Schertl, D., Weigelt, G., Baffa, C., Chelli, A., Petrov, R., & Robbe-Dubois, S. 2013, *A&A*, 555, A24

Ohnaka, K., Weigelt, G., & Hofmann, K.-H. 2016, *A&A*, 589, A91

Ohnaka, K., Weigelt, G., & Hofmann, K.-H. 2017, *A&A*, 597, A20

Schwarzschild, M. 1975, *ApJ*, 195, 137

Shenoy, D., Humphreys, R. M., Jones, T. J., *et al.* 2016, *AJ*, 151, 51

Smartt, S. J. 2015, *PASA*, 32, 16

Smith, N., Humphreys, R., Davidson, K., *et al.* 2001, *AJ*, 121, 1111

Smith, N., Hinkle, K. H., & Ryde, N. 2009, *AJ*, 137, 3558